Influence of the Valley Surroundings on Valley Wind Dynamics

JUERG SCHMIDLI

Institute for Atmospheric and Climate Science, ETH Zurich, Zurich Switzerland, and National Center for Atmospheric Research, Boulder, Colorado

RICHARD ROTUNNO

National Center for Atmospheric Research, Boulder, Colorado

(Manuscript received 10 May 2011, in final form 17 August 2011)

ABSTRACT

In a recent study, the authors investigated the mechanisms leading to the formation of diurnal along-valley winds in a valley formed by two isolated mountain ridges on a horizontal plain. The main focus was on the relation between the valley heat budget and the valley–plain pressure difference. The present work investigates the influence of the valley surroundings on the evolution of the valley winds. Three valley–plain configurations with identical valley volumes are studied: a periodic valley, an isolated valley on a plain (the former case), and an isolated valley entrenched in an elevated plateau. According to the valley volume argument (topographic amplification factor), these three cases should develop identical temperature perturbations and thus similar along-valley winds. However, substantial differences are found between the three cases, in particular a much stronger daytime up-valley wind and nighttime down-valley wind for the plateau configuration. The analysis demonstrates the importance of the exchange of along-valley momentum between the valley atmosphere and its surroundings and of the upper-level pressure gradient in explaining the differences among the cases. Furthermore, differences in the upper-level pressure gradient are shown to be related to the heat exchange of the air above the valley atmosphere with the surroundings, which is related to larger-scale cross-valley circulations.

1. Introduction

Diurnal mountain winds are a key component of the atmospheric boundary layer over complex terrain. They strongly influence the land surface–atmosphere exchanges of heat, momentum, moisture, and other constituents. The fluxes induced by the slope and valley winds can be much larger than the near-surface turbulent fluxes (e.g., Weigel et al. 2007). The quantification of these exchanges is important for many applications such as air quality studies, numerical weather prediction, and climate modeling (e.g., Rotach et al. 2004, 2008; Gohm et al. 2009). But they also directly influence the characteristics of local weather and climate such as near-surface temperatures, wind speeds, cloudiness, and precipitation (e.g., Egger et al. 2000). Despite the importance of the diurnal mountain winds, there is still some uncertainty regarding the influence of the valley surroundings and the larger-scale plain-to-mountain flow on the dynamics of the valley wind.

The major cause for the development of thermally induced along-valley winds has long been attributed to the valley volume effect, which can be quantified in terms of a topographic amplification factor (TAF; Wagner 1938; Steinacker 1984; McKee and O'Neil 1989). The TAF concept is based on an argument stating that a given amount of energy input (or loss) applied to a valley heats (cools) a smaller volume of air than if the same energy input is applied over a plain, resulting in a larger heating (cooling) rate of the valley atmosphere. The main underlying assumption is that no heat is exchanged with the free atmosphere above the valley. Recently the role of the valley volume effect for the daytime valley wind evolution was questioned by Rampanelli et al. (2004). Schmidli and Rotunno (2010, hereafter SR10) developed a new diagnostic framework and performed idealized numerical simulations to help clarify the role of various

Corresponding author address: Juerg Schmidli, Institute for Atmospheric and Climate Science, Universitaetsstrasse 16, ETH Zurich, CH-8092 Zurich, Switzerland.
E-mail: jschmidli@env.ethz.ch

DOI: 10.1175/JAS-D-11-0129.1

forcing mechanisms (such as the valley volume effect, subsidence heating, and surface sensible heat flux effects) on the diurnal evolution of the along-valley wind. The focus of SR10 was on the different mechanisms affecting the heat budget of the valley. The present paper extends SR10 by reporting on experiments of idealized valley flows for different valley–plain configurations and analyzing the influence of the valley surroundings on the evolution of the along-valley wind.

The valley–plain topography used in SR10 consisted of a valley with a horizontal floor enclosed by two isolated mountain ridges on a horizontal plain. In contrast, the topography used by many previous studies consisted of a valley entrenched in an elevated plateau opening onto a plain (McNider and Pielke 1984; Li and Atkinson 1999; Rampanelli et al. 2004), sometimes also including a sloping valley floor (e.g., Li and Atkinson 1999). An even simpler topography is used by Egger (1990): the valley consists of a box with vertical or sloping sidewalls and the domain does not extend beyond the valley in cross-valley direction. For large-eddy simulation studies of the valley atmosphere the topography is often further simplified to that of an infinitely long valley (e.g., Serafin and Zardi 2010; Catalano and Moeng 2010). These different idealized valley–plain configurations are a reflection of the different dominant valley types in different regions of the world. The configuration chosen by SR10 was inspired by California's Owens Valley, which is formed by the Sierra Nevada range to the west and the White and Inyo Mountains to the east. Other configurations may be more typical for valleys in the Intermountain West region or in the European Alps. Regarding the computational setup, SR10 used a large computational domain with periodic lateral boundary conditions. Most previous studies were conducted with a smaller domain and using some type of open lateral boundary conditions. While open lateral boundary conditions may induce artificial sources of mass and heat, periodic lateral boundary conditions guaranty that the boundary conditions respect the conservation of mass and heat.

As shown in SR10 and discussed in more detail in the present study, the valley surroundings can influence the evolution of the along-valley wind in three distinct ways: first, through a modification of the valley heat budget and the low-level along-valley pressure gradient; second, through a modification of the ridge-top along-valley pressure gradient as a result of its influence on the heat exchange above the valley; and third, through its influence on the exchange of along-valley momentum between the valley and its surroundings. The first mechanism was the focus of SR10. The latter two are the focus of the present study.

Some of these forcings external to the valley atmosphere may be the direct result of the along-valley circulation itself. It is clear, however, that larger-scale thermally induced flows such as plain-to-mountain flows oriented in cross-valley and along-valley direction, such as plain-to-basin flows (De Wekker et al. 1998) or plain-to-plateau flows (Zängl and Chico 2006), may also contribute to the three forcing mechanisms.

Finally, we should stress that we only consider pure thermally induced flows. Other external influences such as larger-scale synoptic pressure gradients and momentum exchange induced by larger-scale synoptic flows (Whiteman and Doran 1993; Schmidli et al. 2009) are not considered. Also our main focus is on the evolution of the mean valley wind and not on the local details. The focus on the mean wind is motivated by the finding that its evolution is quite robust with respect to modeling choices (Schmidli et al. 2011), and that the local evolution of the flow is often highly correlated to the evolution of the mean along-valley wind (Weigel et al. 2007; Schmidli et al. 2011). In summary, our goal is to provide a comprehensive analysis of the influence of the valley surroundings on the evolution of the mean along-valley wind.

The plan of this paper is as follows. Section 2 reviews some theoretical considerations regarding along-valley momentum and the along-valley pressure gradient. In section 3, we briefly summarize the numerical setup of our experiments; in particular, we introduce the three valley–plain topographies to be used in the present study. It should be noted that the valleys per se have identical dimensions (and geometry) for all cases considered. Thus, according to the TAF concept, one would expect the development of identical temperature perturbations and similar along-valley winds. This is, however, not what is found. Section 4 reports on the influence of the different valley–plain topographies on the diurnal evolution of the valley wind system and section 5 analyzes the mechanisms through which the valley surroundings influence the valley flow evolution. Section 6 summarizes the results.

2. Theory

As in SR10, we consider a straight valley of uniform depth h with a horizontal floor, closed at one end and open toward a plain at the other end (see Fig. 1 for an example). Then the momentum equation for the along-valley wind at height z is (SR10)

$$\frac{\partial v}{\partial t} = -\frac{1}{\rho}\frac{\partial p_l}{\partial y} - \frac{1}{\rho}\frac{\partial p_{\text{top}}}{\partial y} - \mathbf{v}\cdot\nabla v - \frac{1}{\rho}\nabla\cdot\mathbf{T}_v, \qquad (1)$$

where v is the along-valley velocity; ρ is the density; y is the Cartesian coordinate in the along-valley direction;

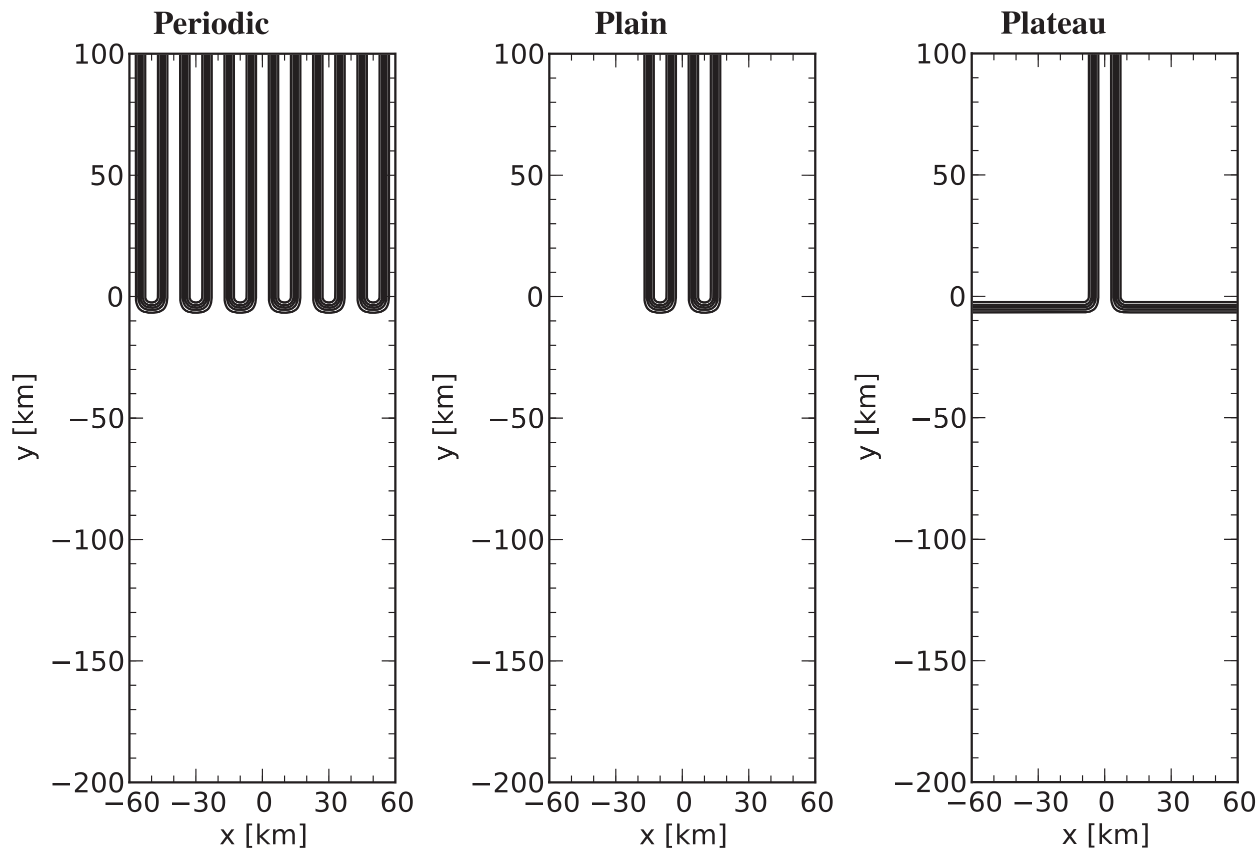

FIG. 1. Height contours of topography and computational domain adopted for the three valley–plain configurations described in the text.

the vector $\mathbf{T}_v$ is the turbulent flux of along-valley momentum; p_{top} is the pressure at the height of the mountain ridge top, $p_{\mathrm{top}} = p(x, y, z = h)$; and p_l is the lower-level contribution to the pressure at height z (i.e., $p = p_l + p_{\mathrm{top}}$). For hydrostatic flow, p_l is fully determined by the temperature distribution θ between the height z and the top of the valley atmosphere h.

To arrive at a tendency equation for the bulk flow, the momentum equation is integrated over the valley volume V. The volume-averaged density-weighted momentum equation is

$$\underbrace{\frac{1}{M}\int_V \rho \frac{\partial v}{\partial t}\,dV}_{\text{NET}} = \underbrace{-\frac{1}{M}\int_V \frac{\partial p}{\partial y}\,dV}_{\text{PGR}} \underbrace{-\frac{1}{M}\int_{A_S} \rho u_*^2 \frac{v}{|\mathbf{v}|}\,dS}_{\text{SFC}} \underbrace{-\frac{1}{M}\int_V \rho \mathbf{v}\cdot\nabla v\,dV}_{\text{ADV}} \underbrace{-\frac{1}{M}\int_{A_A} \mathbf{T}_v\cdot\mathbf{n}\,dS}_{\text{TRB}}, \qquad (2)$$

where M is the total mass of air in the control volume and u_* is the surface friction velocity. Equation (2) follows from the integration of (1) and by using Gauss' theorem to convert the resulting volume integral of the turbulent flux divergence term into a corresponding surface integral and by decomposing the resulting surface integral of the turbulent momentum fluxes into a land surface part A_S and an atmospheric part A_A. In words, the density-weighted volume-averaged net along-valley wind speed tendency (NET) is equal to the sum of the contributions due to the along-valley pressure gradient (PGR), the surface friction (SFC), total advection (ADV), and turbulent momentum flux through A_A (TRB).

In the case of a valley with a constant cross-valley section, the pressure gradient term can be expressed as

$$\underbrace{-\frac{1}{M}\int_{A_{xz}} \Delta p_v(x,z)\,dS}_{\text{PGR}}, \qquad (3)$$

where Δp_v is the pressure difference between the two sides of the control volume. In SR10, the pressure gradient force (at the surface) is approximated by the valley–plain surface pressure difference along the valley axis

$\Delta p_{\rm sfc} = p(0, y_v, 0, t) - p(0, y_p, 0, t)$ and it is shown that it can be expressed as

$$\Delta p_{\rm sfc} = -\frac{g}{\theta_0}(Q_v^n - Q_p^n) + \Delta p_{\rm top}, \quad (4)$$

where Q_v^n and Q_p^n denote the (normalized) net heat input into the valley and plain control volume, respectively, and $\Delta p_{\rm top} = p(0, y_v, h, t) - p(0, y_p, h, t)$ is the valley–plain pressure difference at mountain ridge-top height. In other words, the valley–plain surface pressure difference is determined by the difference in the heating histories of the valley and plain control volume. However in the context of explaining the evolution of the mean along-valley flow in the valley control volume, $\Delta p_{\rm sfc}$ alone might not be sufficient; rather, it can be expected that the volume-averaged pressure gradient [(3)] will be better approximated by some combination of $\Delta p_{\rm sfc}$ and $\Delta p_{\rm top}$. Moreover, the other terms in (2) might also be important for explaining the valley wind evolution. In section 4b different valley–plain topographies are compared in terms of the approximate bulk approach [(4)], while in section 5 the evolution of the different cases is analyzed using the exact momentum budget [(2)].

3. Numerical setup

The numerical setup of the simulations, apart from the topography, is identical to the one described in SR10 and detailed information can be found there. For convenience we summarize the main aspects of the setup after introducing the new valley–plain geometries. To investigate the influence of the valley surroundings on the evolution of the along-valley wind, we introduce the three valley–plain configurations with horizontal valley floors as shown in Fig. 1. The periodic configuration (hereafter PERIODIC) consists of an infinite number of parallel valleys opening onto a common plain. The plain configuration (hereafter PLAIN)—which is identical to SR10—denotes a valley formed by two isolated mountain ridges on a horizontal plain. The plateau configuration (hereafter PLATEAU) consists of a valley cut into a large-scale plateau. As mentioned in the introduction, the dimensions (and geometry) of the valleys per se are identical for all three configurations. As in SR10, the topographies are the product of two simpler ones. The analytic expression for the topographies is given by

$$z = h(x, y) = h_p h_x(x) h_y(y), \quad (5)$$

where

$$h_y(y) = \begin{cases} 0 & y \le -S_y \\ \dfrac{1}{2} + \dfrac{1}{2}\cos\left(\pi \dfrac{y}{S_y}\right) & -S_y < y < 0 \\ 1 & y \ge 0 \end{cases} \quad (6)$$

is identical for all three configurations. The only difference is in the cross-valley direction. The analytic expression for h_x is given by

$$h_x(x) = \begin{cases} 0 & |x| \le X_1 \\ \dfrac{1}{2} - \dfrac{1}{2}\cos\left(\pi \dfrac{|x| - X_1}{S_x}\right) & X_1 < |x| < X_2 \\ 1 & X_2 \le |x| \le X_3 \end{cases} \quad (7)$$

for PERIODIC and PLATEAU (with an appropriate continuation for PERIODIC) and by

$$h_x(x) = \begin{cases} 0 & |x| \le X_1 \\ \dfrac{1}{2} - \dfrac{1}{2}\cos\left(\pi \dfrac{|x| - X_1}{S_x}\right) & X_1 < |x| < X_2 \\ 1 & X_2 \le |x| \le X_3 \\ \dfrac{1}{2} + \dfrac{1}{2}\cos\left(\pi \dfrac{|x| - X_3}{S_x}\right) & X_3 < |x| < X_4 \\ 0 & |x| \ge X_4 \end{cases} \quad (8)$$

for PLAIN.

As in SR10, the simulations are initialized from an atmosphere at rest with a constant stratification corresponding to a Brunt–Väisälä frequency of about 0.011 $\rm s^{-1}$. The model is integrated for up to 40 h starting from sunrise which is at 0600 local time (LT). The surface sensible heat flux driving the thermally induced circulations is determined by the complete (dry) model physics—that is, by the interaction of the radiation scheme with the land surface scheme and atmospheric dynamics. As in SR10, the numerical simulations have been carried out using the Advanced Regional Prediction System (ARPS) model (Xue et al. 2000, 2001). The computational domain for the all three configurations is 300 km in the along-valley direction and 120 km in the cross-valley direction. The horizontal grid spacing is 1 km and the vertical grid spacing varies from 20 m near the surface to a maximum of 200 m above 2 km. The lateral boundary conditions are periodic in the cross-valley direction and free-slip wall conditions are imposed in the along-valley direction. This choice minimizes the required computational resources, as doubly periodic boundary conditions would require a computational domain of double the current size in the along-valley direction. Also, as mentioned in the introduction, periodic lateral boundary conditions and free-slip wall boundary conditions ensure that no artificial sources of mass and heat are introduced at the boundaries. In addition to the three-dimensional valley–plain topographies, we also carried out simulations for two-dimensional valley geometries, corresponding to infinitely long valleys, with identical cross sections to those introduced above. For these two-dimensional valleys we have $h_x(x)$ as above and $h_y(y) = 1$.

4. Diurnal flow evolution

In this section we document the diurnal evolution of the valley wind system in terms of its spatial structure and the temporal evolution of the mean along-valley wind. Detailed information on the complete diurnal cycle for PLAIN can be found in SR10; here we focus on the differences between the configurations.

a. Spatial structure

A snapshot of the well-developed daytime flow in a cross-valley plane located 20 km up valley from the valley entrance and in an along-valley plane located at the valley center for the three configurations is shown in Fig. 2. The cross-valley circulations are well established in all three cases with upslope flows on the valley sidewalls, flow convergence over the mountain ridges (PERIODIC, PLAIN), and weak subsiding motion over the center of the valley. Because of the setup, the flow pattern is symmetric with respect to the valley center for all three cases; in addition, it is also symmetric with respect to the mountain ridge for PERIODIC. For PLAIN the larger-scale plain-to-mountain flow has moved the area of upslope-flow convergence 1.5 km toward the valley center. For PLATEAU the cross-valley extent of the cross-valley circulation is much larger.

The core of the along-valley flow has attained a speed of over 6 m s^{-1} for PLATEAU and over 4 m s^{-1} for the other two cases. Significant differences are notable in the spatial pattern of the along-valley flow. The up-valley flow is advected to higher altitudes over the slopes for PLAIN than for the other two cases; this might be related to the return flows. No significant return flow is visible for PLAIN; for the other two cases a return flow larger than 2 m s^{-1} is visible above the valley. Substantial differences in the structure of the along-valley flow can also be seen in the along-valley sections located on the valley axis. The magnitude and horizontal extent of the up-valley flow is largest for PLATEAU. Also, the location of the maximum up-valley flow differs between the cases. It remains close to the valley entrance for PERIODIC, but it moves about 20 km up the valley between 1200 and 1800 LT for PLAIN and PLATEAU. A strong return flow along the valley center axis is visible for PERIODIC. The quasi-periodic along-flow pattern upstream of the valley entrance, most visible for PLAIN, is likely related to the ARPS turbulence scheme and unresolved cellular motions in the convective boundary layer. Other models do not show such quasi-periodic patterns (Schmidli et al. 2011).

Figure 3 shows a snapshot of the well-developed nighttime flow. The downslope flows are much shallower than upslope flows. The along-valley wind is more confined to the valley core. The down-valley flow is much stronger and deeper for PLATEAU. The maximum wind speeds at the valley exit attain 8 m s^{-1} for PERIODIC, but 12 m s^{-1} for PLATEAU. The maximum depth of the layer with significant down-valley flow (>2 m s^{-1}) is almost twice as deep for PLATEAU in comparison to PERIODIC. As during the daytime, significant upper-level return flows over the valley are observed only for PERIODIC and PLATEAU. Thus, the different surroundings lead to a qualitatively different return flow for PLAIN, for both day and night. Averaging the flow over the up-valley and down-valley flow period, respectively, it is found that the maximum of the return flow for PLAIN occurs at lower altitudes and near the lateral boundaries of the domain. These maxima are found at about 2 km AGL during the day and at 1 km AGL during the night (not shown). Because of geometrical constraints such a low-level return flow is not possible for the other two cases.

A quantitative comparison of the along-valley variation of the mean-along valley wind for the three configurations is shown in Fig. 4. The daytime up-valley wind for PLATEAU is about twice as strong as the up-valley wind of PERIODIC and still substantially stronger than PLAIN. For the nighttime down-valley wind the difference between the three configurations is even larger. Maximum wind speeds differ by about a factor of 2 between PERIODIC and PLAIN and again by a factor of 2 between PLAIN and PLATEAU.

b. Evolution of the mean along-valley wind

The evolution of the mean along-valley wind, averaged over the first 20 km and over the entire valley, and the valley–plain pressure difference at the surface and at mountain-ridge height are shown in the left column in Fig. 5. Not surprisingly, the along-valley wind and the pressure gradient forcing are quite closely correlated for all configurations. There is a notable asymmetry between the evening and the morning transition (on the second day). During the evening transition the pressure gradient forcing switches sign 3–4 h before the along-valley wind. During the morning transition the change of sign occurs almost at the same time. Surprisingly, the difference among the configurations in the valley–plain

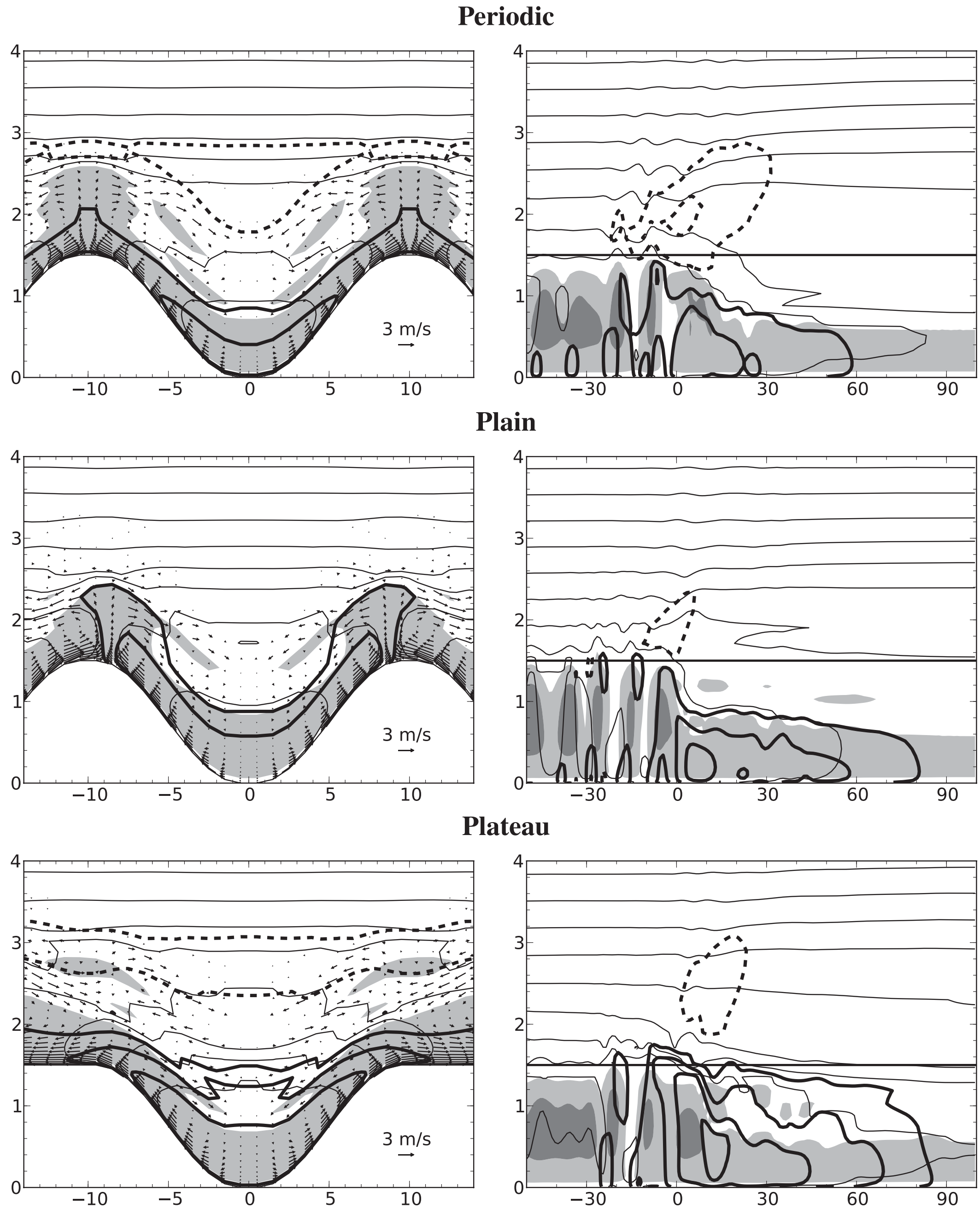

FIG. 2. Cross-valley sections at $y = 20$ km and along-valley sections at $x = 0$ km of the flow at 1500 LT showing wind vectors, along-valley flow (thick contours; contour interval = 2 m s^{-1}; negative values are dashed), potential temperature (contour interval = 1 K), and eddy diffusivity (shading; 10 and 50 m^2 s^{-1}). The axis units are kilometers. Wind vectors with magnitude smaller than 0.2 m s^{-1} are not shown. (right) The horizontal line refers to the ridge-top height.

surface-pressure differences Δp_{sfc} is substantially smaller than the difference in the strength of the along-valley wind. Note that the upper-level valley–plain pressure difference during the daytime is positive for PERIODIC, almost zero for PLAIN, and negative for PLATEAU. The evolution of the surface sensible heat flux in the valley and over the plain is shown in the right column in Fig. 5. The evolution of the surface heat flux is very similar for all configurations, except during the second half of the night. After midnight, the surface cooling over the plain increases to about -30 W m^{-2} for PERIODIC, to -50 W m^{-2} for PLAIN, but to almost -80 W m^{-2} for

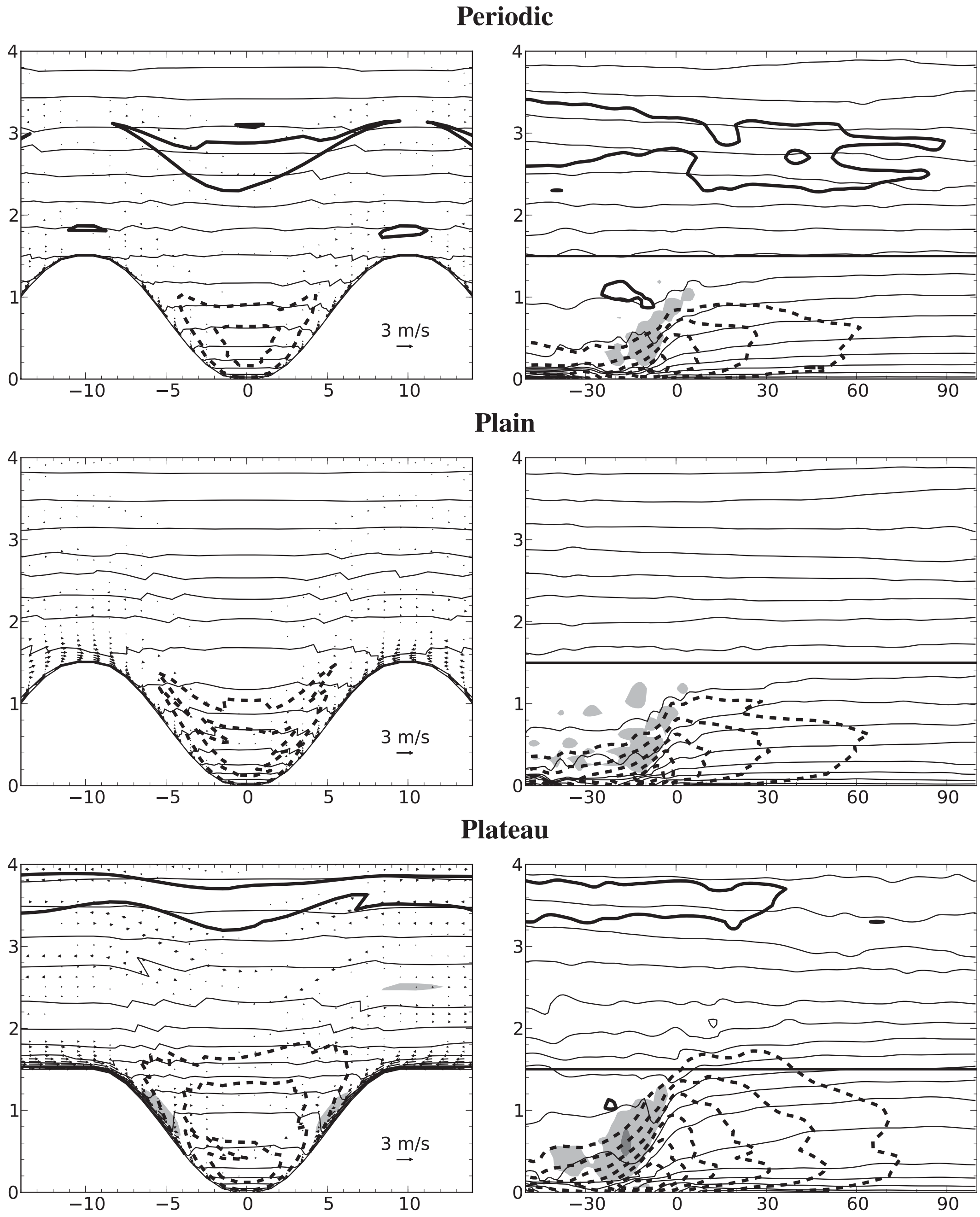

FIG. 3. As in Fig. 2, but for 0600 LT on the second day.

PLATEAU. This implies that the feedback of the flow on the surface sensible heat flux is very small most of the time, but large after midnight over the plain.

5. Analysis of valley wind formation

In section 2, we reviewed the different mechanisms leading to an along-valley acceleration of the flow. Next, we examine in more detail the processes that contribute to the differences in the along-valley wind evolution for the three topographic configurations.

a. The valley heat budget and along-valley pressure gradients

Time series of the heat budget components for the valley control volume for the three configurations are shown in the left column in Fig. 6. As expected from Fig. 5,

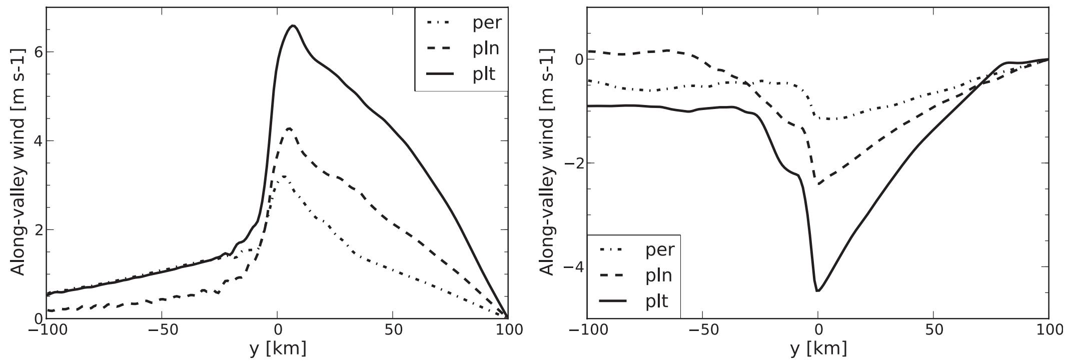

FIG. 4. Along-valley variation of the mean along-valley wind for (left) daytime at 1500 LT and (right) nighttime at 0300 LT. The along-valley wind is averaged over the width and depth of the valley cross section. The abbreviations refer to PERIODIC (per), PLAIN (pln), and PLATEAU (plt).

the diurnal temperature tendencies due to the surface sensible heat flux (shf) are very similar for all three cases. The contribution from the radiation flux divergence (rad) is small during the day but comparable to the sensible heat flux (shf) contribution during the night. As the heat flux is similar for all three cases, so is the total diabatic forcing (shf + rad). The most significant differences among the cases are found for the advective tendencies (adv). The stronger the daytime up-valley wind, the larger the cooling tendency due to advection. During the nighttime there are not only quantitative but also qualitative differences in the evolution of the advective tendencies between PLATEAU and the other two cases. The temperature tendencies due to turbulent vertical mixing (tmix) and computational horizontal mixing (cmix) are small and of similar amplitude for all three cases.

A closer view of the advective tendencies and their decomposition into the heat flux through the valley top (top) and through the valley entrance (mouth) is shown in the right column in Fig. 6. During the daytime the advective temperature tendencies are negative because of the import of cooler air through the valley mouth and the export of warmer air through the valley top. The total advective tendencies remain negative during the evening transition, but they switch sign around midnight. For PERIODIC and PLAIN, the total advective tendencies remain positive throughout the remainder of the night and the morning until the onset of the up-valley wind (import of warmer air through the valley top and export of cooler air through the valley mouth). For PLATEAU the advective tendency becomes negative again after 0200 LT. This is due to the import of cold air—cooled over the high plateaus—through the valley top and the export of relatively warm air through the valley mouth. The latter is the result of the significantly deeper down-valley flow for PLATEAU. Because of the deep flow, the average temperature of the air flowing out of the valley is warmer than the valley-mean temperature.

Most of the time, the differences in the evolution of the valley heat budget among the three configurations is relatively small and they cannot explain the large difference in along-valley wind speed. If anything, the stronger along-valley winds reduce the temperature contrast between the valley and the plain.

It is clear from the local momentum equation [(1)] that the bulk view of the valley wind—comparing a valley and plain control volume—cannot be expected to provide a complete characterization of the forcings, as spatial variations within the control volumes are neglected. Figure 7 compares the along-valley variation of the ridge-top pressure p_{top} and of the cross-valley mean potential temperature for the three configurations. As expected from the heat budgets, the daytime temperatures in the valley (1500 LT) are highest for PERIODIC and lowest for PLATEAU. Note the large difference in ridge-top pressure among the configurations with higher pressure over the valley for PERIODIC and lower pressure over the valley for PLATEAU. Assuming that the flow is hydrostatic, this implies higher upper-level temperatures for PLATEAU and lower upper-level temperatures for PERIODIC in comparison to PLAIN.

During the evening transition (2200 LT) there is a particularly large along-valley temperature gradient for PLATEAU, despite relatively small differences in the bulk heat budget between PLATEAU and the other cases (Fig. 6). In addition, there is a substantial ridge-top pressure gradient for PLATEAU. Together these two factors lead to a strong pressure gradient at lower elevations, which helps explain the rapid transition from up-valley to down-valley flow for PLATEAU. Because of the weaker daytime warming and the strong cooling during the evening transition, the nighttime temperature

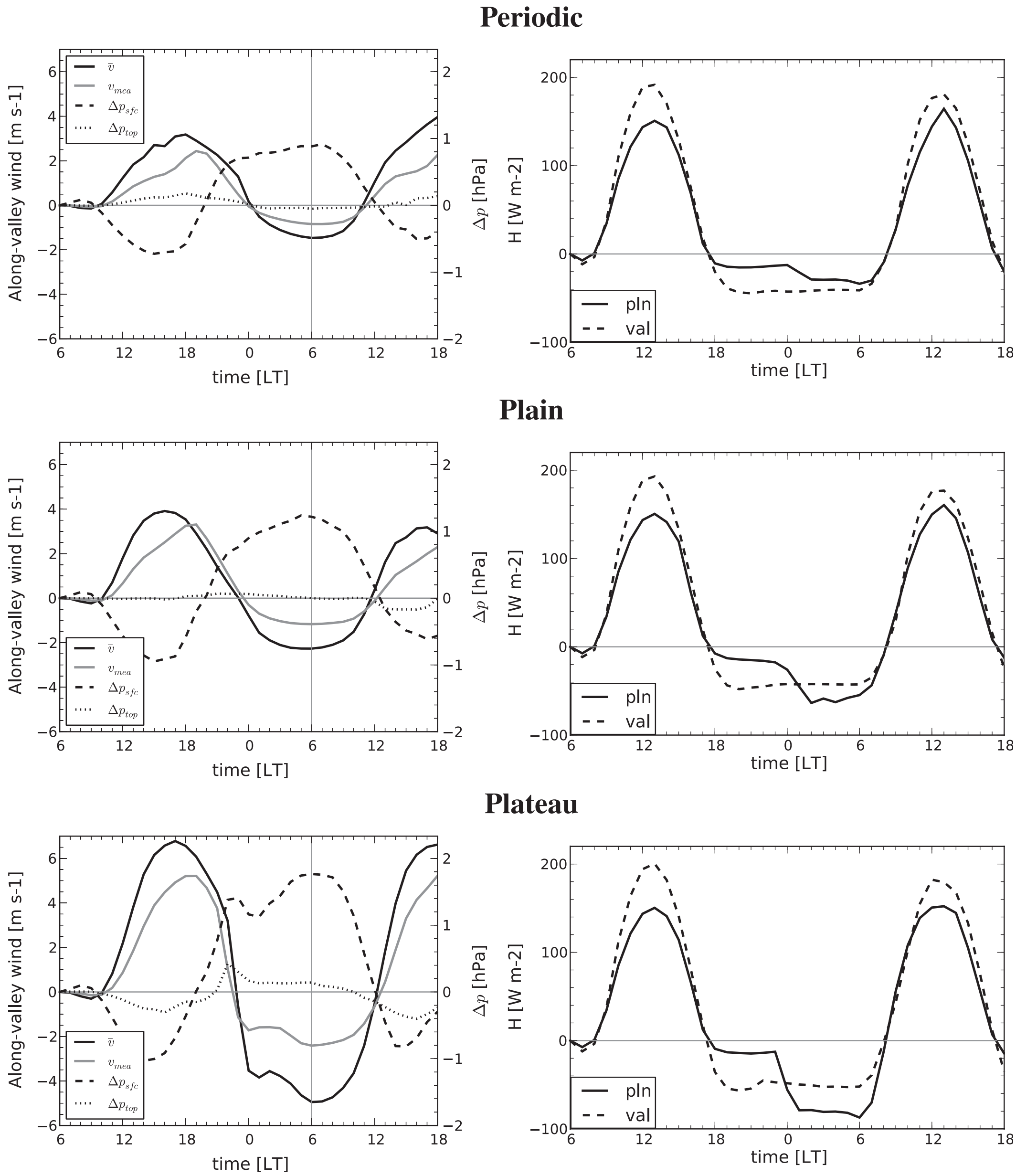

FIG. 5. Time series of (left) mean along-valley wind and along-valley pressure difference and (right) surface sensible heat flux. The pressure difference at the surface and the ridge-top height is taken between $y = -40$ km and $y = 80$ km. The mean along-valley wind is averaged over $y = 0$–20 km ($\overline{v}$) and over the entire valley (v_{mea}). The surface sensible heat flux is shown for a control volume over the plain and the valley.

(0300 LT) is considerably lower for PLATEAU. The nighttime ridge-top pressure gradients are small for all three cases.

In summary, the large difference in the ridge-top pressure gradient during the day and evening transition and the substantial difference in valley temperature during the evening transition and the night are prime candidates for explaining the differences in the diurnal evolution of the along-valley wind.

b. The valley momentum budget

Next, we examine in more detail all the processes that contribute to the formation of the mean along-valley wind. Time series of the momentum budget components (section 2) integrated over the valley volume are shown in the left column in Fig. 8. As expected from the findings of the previous section, the diurnal amplitude of the pressure gradient forcing increases significantly from

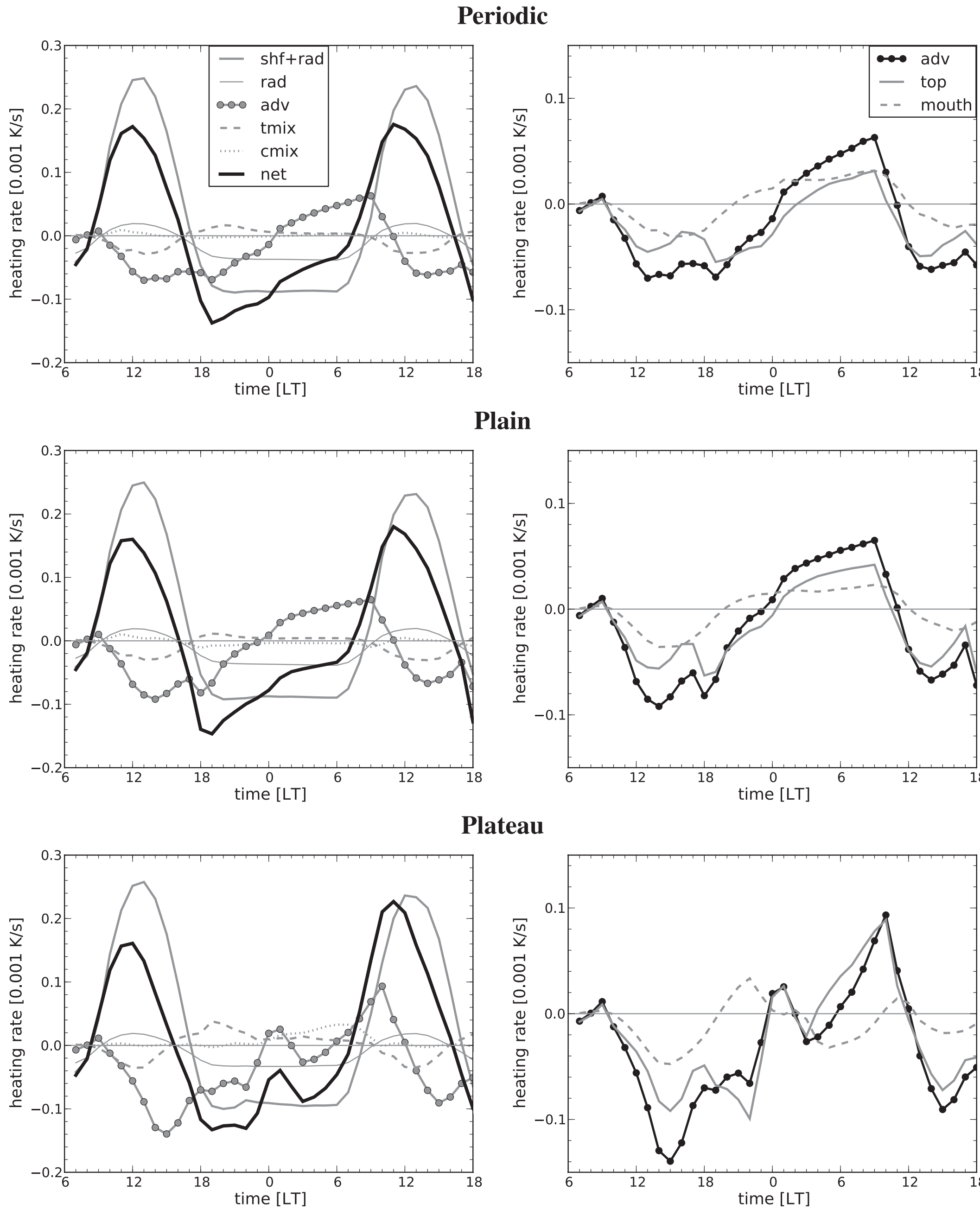

FIG. 6. Time series of the heat budget components (left) averaged over the entire valley and (right) decomposition of the advective tendency. The abbreviations refer to surface sensible heat flux (shf), radiation flux divergence (rad), advection (adv), turbulent vertical mixing (tmix), computational horizontal mixing (cmix), the net tendency (net), valley top (top), and valley mouth (mouth).

PERIODIC to PLAIN and from PLAIN to PLATEAU. There is a distinct asymmetry between the daytime and the nighttime evolution. During the daytime, the pressure gradient forcing follows the evolution of the surface sensible heat flux (Fig. 5) with a delay of 1–2 h. During the evening transition the forcing becomes strongly negative, and then remains approximately constant during the early morning hours until after sunrise. Note the much stronger deceleration during the evening transition for PLATEAU. It is clear that this strong forcing cannot be fully explained by differences in the heat budget for valley-mean temperatures (Fig. 6), and that strong along-valley gradients of temperature and pressure within and above the valley (Fig. 7) play a major

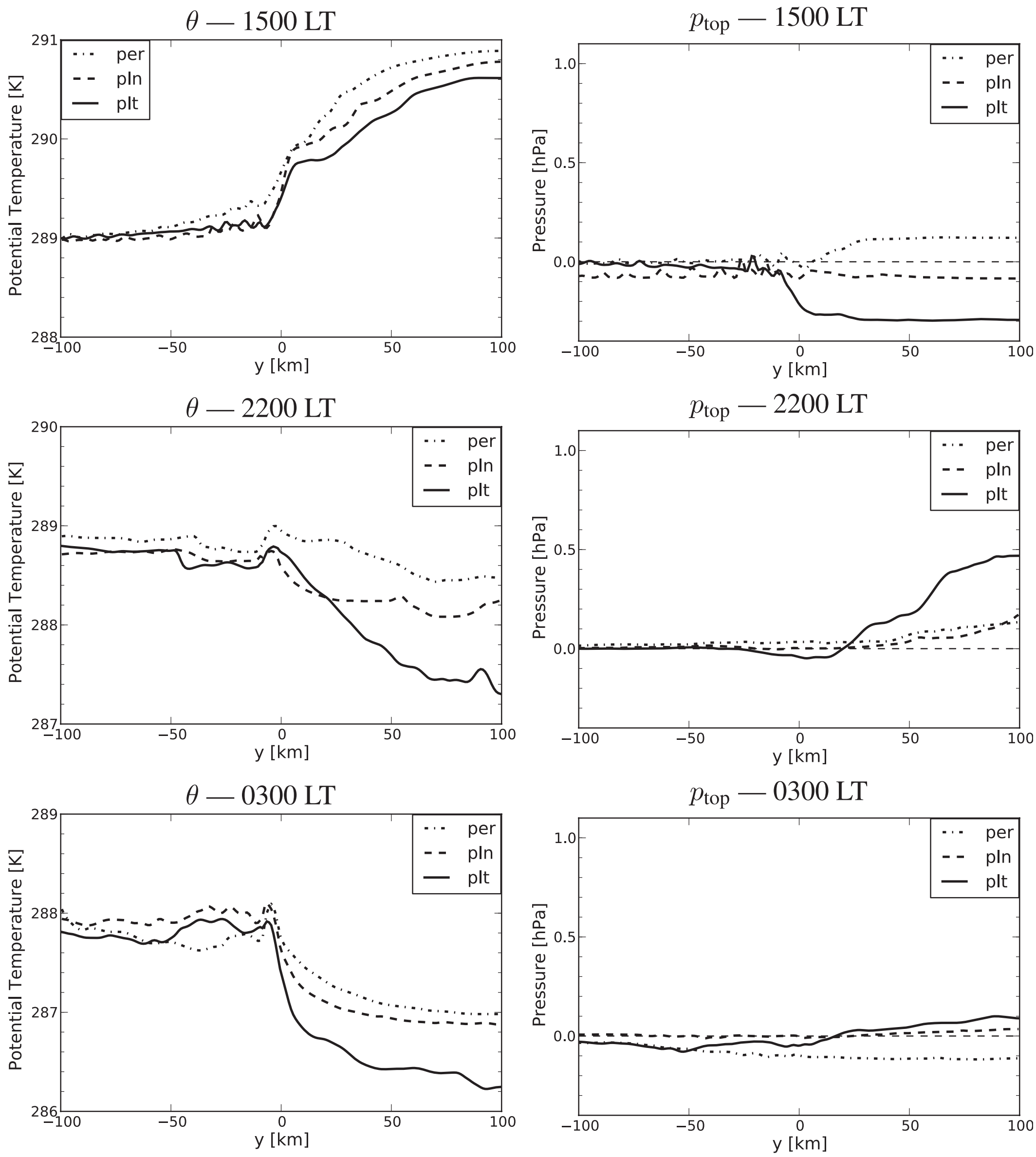

FIG. 7. Along-valley (left) potential temperature and (right) pressure variation for the three experiments at three different times (daytime, transition to down-valley flow, nighttime). Potential temperatures are averaged in cross-valley direction and from the surface to ridge-top height; pressure is at ridge-top height. Axes for pressure are chosen such that $p_{top} = 0$ at $y = -200$ km.

role for the differences between PLATEAU and the other two cases. The momentum tendency due to surface friction exhibits a large day–night asymmetry. During the day surface friction is large and negative, retarding the along-valley flow, during the night the effect of surface friction on the along-valley flow is negligible. This asymmetry is caused by the difference in atmospheric stratification between the day and the night. The large stability during the nighttime strongly reduces the exchange of momentum between the atmosphere and the surface.

The momentum tendency due to the advection of along-valley momentum is most significant during the night. For all three cases, there is an approximate equilibrium between the pressure gradient and the advection term during the later part of the night. During this period the net acceleration is therefore close to zero and the mean along-valley flow is almost steady (Fig. 5), in particular for PERIODIC and PLAIN. Large differences among the cases are found during the daytime and the evening transition. During this period, the advection

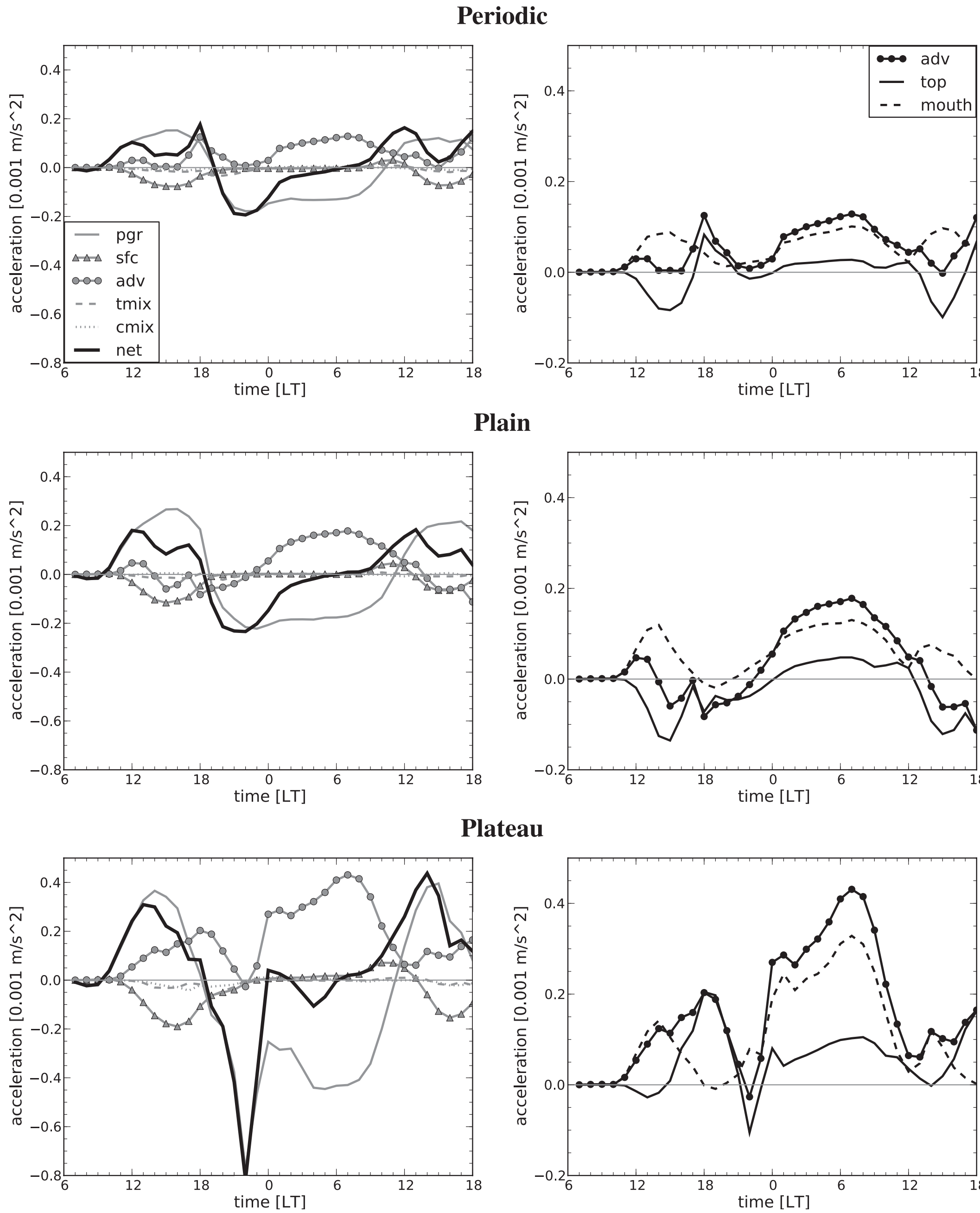

FIG. 8. Time series of the along-valley momentum budget components (left) averaged over the entire valley and (right) decomposition of the advective tendency.

term is small for PERIODIC and PLAIN, with the exception of the positive peak at 1800 LT for PERIODIC. For PLATEAU, on the other hand, the advection term is large and positive during the day and first part of the evening transition (until 2200 LT).

A decomposition of the advective tendencies into fluxes through the valley top and through the valley entrance is shown in the right column in Fig. 8. The momentum tendency due to advective transport through the valley entrance is positive for day and night. During the daytime the along-valley wind imports high-momentum air into the valley; during the nighttime it exports air with high negative (down-valley) momentum out of the valley. The momentum exchange through the valley top leads to a deceleration of the along-valley flow for PERIODIC and PLAIN as high-momentum air is exported out of the valley during the up-valley flow regime and low-momentum air is imported into the valley during the down-valley flow regime. For PLATEAU, on the other hand, the daytime mean up-valley flow is accelerated because of the export of lower-momentum air through the top of the control volume.

In summary, the large differences in the evolution of the along-valley wind between PLATEAU and the other two cases result mainly from differences in the evolution of the pressure gradient forcing and the advective momentum exchange between the valley and its surroundings. During the nighttime, the pressure gradient term is the dominant source of difference among the cases, during the daytime, both terms are of similar importance.

c. The larger-scale cross-valley circulation, temperature anomalies, and the upper-level pressure gradient

As previously mentioned, the hydrostatic relation implies that the differences in the upper-level along-valley pressure gradients p_{top} are caused by differences in the upper-level temperature distribution between the three configurations. To gain further insight into the processes responsible for the differences, the heat budgets for an extended valley volume for the three cases and the three corresponding two-dimensional ''infinite valley'' cases are compared in Fig. 9. The control volume considered reaches from the surface to a height of 3 km AGL. The two-dimensional runs nicely illustrate the influence of the extended cross-valley circulation. For PLAIN, the larger-scale (cross-valley) plain-to-mountain flow leads to advective cooling between 1200 and 2400 LT, with a maximum in the afternoon. For PLATEAU the larger-scale valley-to-plateau circulation leads to significant warming of the control volume during the daytime and the flow of cold plateau air into the valley leads to a strong cooling peak around midnight. Note that the advective tendencies for the extended volume are primarily the result of heat exchange across the lateral boundaries, and not the top surface, of the control volumes.

Based on the two-dimensional cases, the influence of the larger-scale cross-valley circulations on the heat budgets of the three-dimensional runs can clearly be seen. Total advective cooling during the (daytime) up-valley flow regime is larger for PLAIN than for PERIODIC because of the additional cooling arising from the cross-valley plain-to-mountain flow and the stronger along-valley wind. On the other hand, daytime total advective cooling is much reduced for PLATEAU in comparison to the other two cases because of the warming induced from the larger-scale valley-to-plateau circulation, despite a much stronger up-valley wind. PLATEAU experiences two cooling peaks due to advection. The first at 2200 LT is associated with the export of warm valley air by the remaining up-valley flow and the import of cold plateau air by very shallow downslope flows. The second peak at 0300 LT is related to stronger and deeper downslope flows associated with the larger-scale valley–plateau circulation, as is the peak at 0000 LT in the corresponding two-dimensional case.

The relative insensitivity of the cross-valley circulation to the along-valley flow is further illustrated in Fig. 10. The figure compares the daytime cross-valley flow at $y = 20$ km for the three-dimensional and two-dimensional topographies. It can be seen that the larger-scale cross-valley circulation is very similar for the corresponding two-dimensional and three-dimensional topographies, such as the plain-to-mountain flow for the plain cases and the valley-to-plateau circulation for the plateau cases.

Figure 11 shows vertical profiles of temperature on the valley axis ($x = 0$ km) over the plain ($y = -40$ km), within the valley ($y = 80$ km), and for a corresponding infinite valley (2D infinite). It provides further evidence that the vertical temperature distribution near the valley end is primarily determined by the cross-valley circulation and only to a minor degree by the along-valley circulation. For PLATEAU, however, significant differences are found between the 2D and 3D configuration, with somewhat colder temperatures in the upper part of the valley at 1500 LT and significantly colder temperatures at 0600 LT for the 3D configuration. The primary difference between PLATEAU and the other two configurations becomes clear. During the daytime, the cross-valley circulation for PLATEAU leads to a more pronounced warm anomaly attaining higher altitudes. During the nighttime, the combined effect of the cross- and along-valley circulation leads to a more pronounced and significantly deeper cold anomaly. The stronger upper-level temperature anomalies result in larger upper-level pressure gradients and hence a stronger along-valley flow.

6. Conclusions

In the present study we extend our recent work on the basic physical mechanisms governing the formation of thermally induced along-valley winds in mountain valleys, reported in SR10, by investigating the role of the valley surroundings on the evolution of the valley wind. For this purpose we carried out numerical simulations of thermally driven flows over three different idealized valley–plain topographies. The three cases differ only with respect to the surroundings of the valley; the valley itself is identical for all cases. Thus, according to the

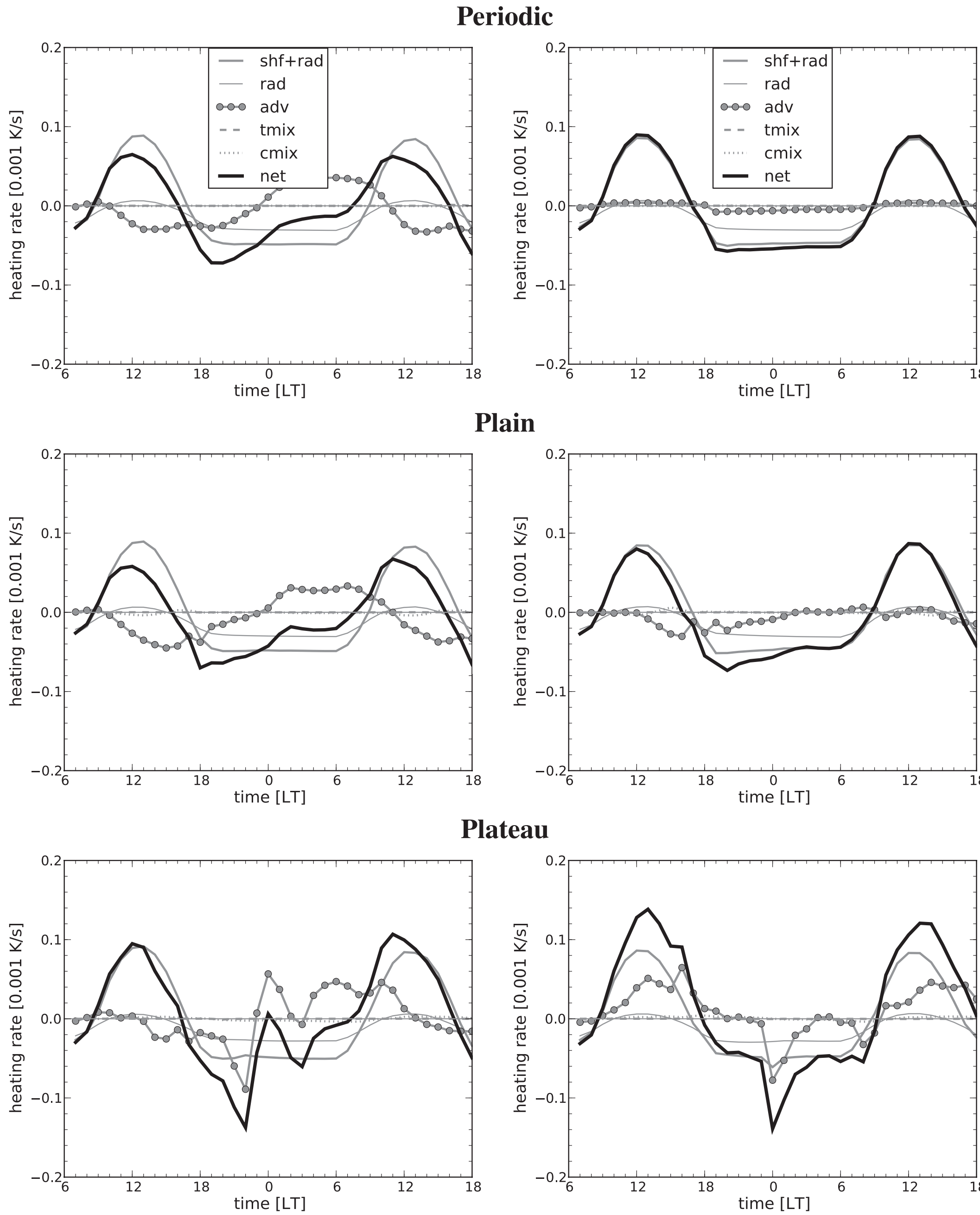

FIG. 9. Time series of the heat budget components averaged over the entire valley for an extended valley control volume reaching from the surface to an altitude of 3000 m, for (left) the 3D plain–valley topographies and (right) the corresponding 2D topographies (i.e., ''infinite valleys'').

TAF argument, the three cases should develop identical temperature perturbations and thus similar along-valley winds.

However, large differences in along-valley wind speeds are simulated. Both the daytime up-valley and the nighttime down-valley wind are about twice as strong for the valley surrounded by an elevated plateau in comparison to the case of a periodic valley and an isolated valley on a plain. During the daytime the elevated plateau acts as an elevated heat source, which leads to upper-level warming over the valley and hence a stronger along-valley pressure gradient and a stronger up-valley wind. During the nighttime, the situation is reversed: the elevated plateau becomes a source of cold air, thus strengthening the

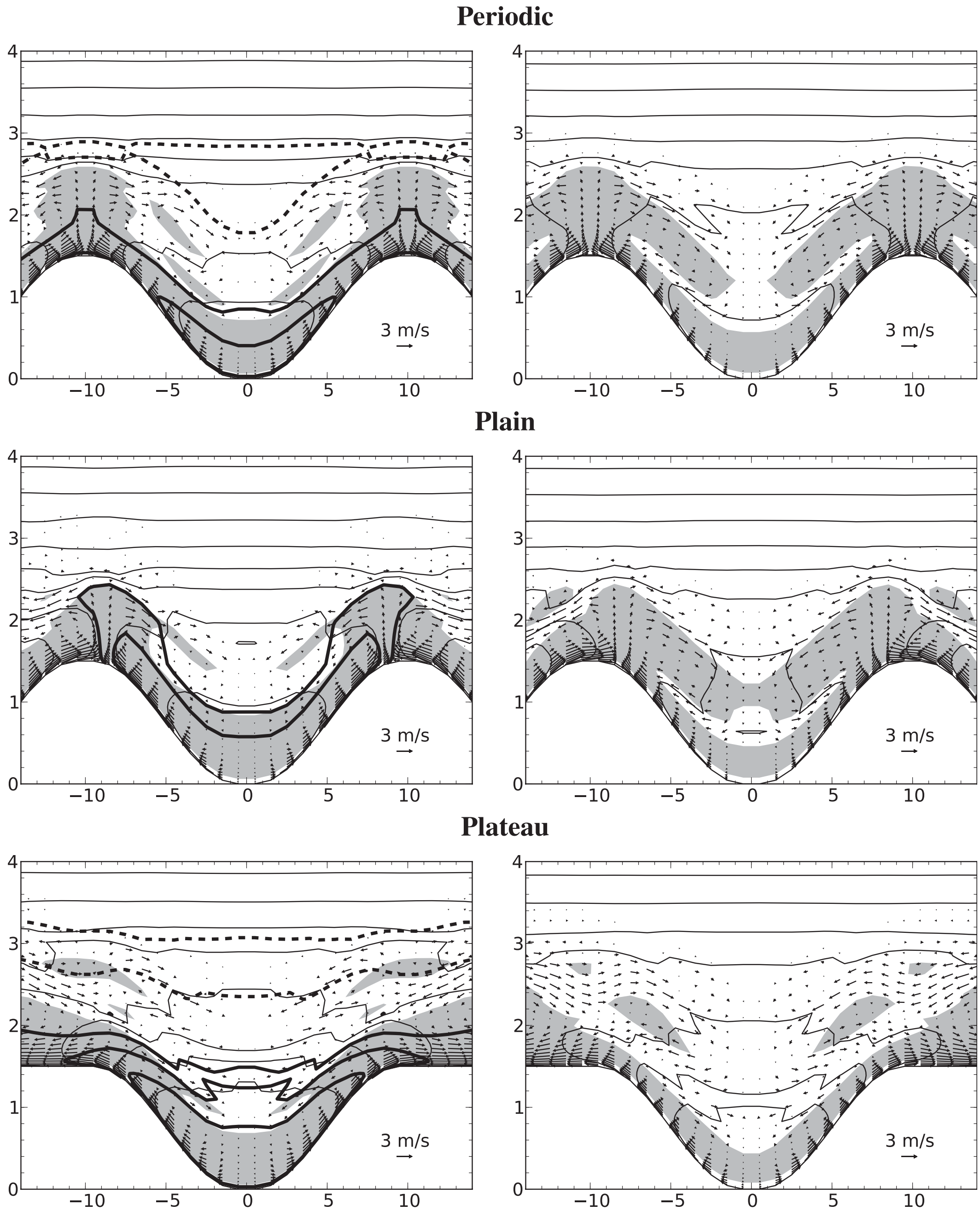

FIG. 10. Cross-valley sections of the flow at 1500 LT at $x = 20$ km as in Fig. 2, for (left) the 3D plain–valley topographies and (right) the corresponding 2D topographies (i.e., infinite valleys).

down-valley flow. Finally, during the evening transition differential advection of cold air results in large along-valley gradients of temperature and pressure within the valley itself.

More generally, the analysis shows that the influence of the surroundings on the evolution of the along-valley wind is transmitted primarily through the upper-level pressure distribution and advective momentum exchange between the valley and its surroundings. The influence of the surroundings on the mean heat budget of the valley itself, the focus of the TAF concept, is quite small. The analysis demonstrates the potential importance of the upper-level pressure distribution, of valley–atmosphere momentum exchange, and of local along-valley gradients of temperature and pressure within the valley volume—three factors not included in the TAF concept—in forcing

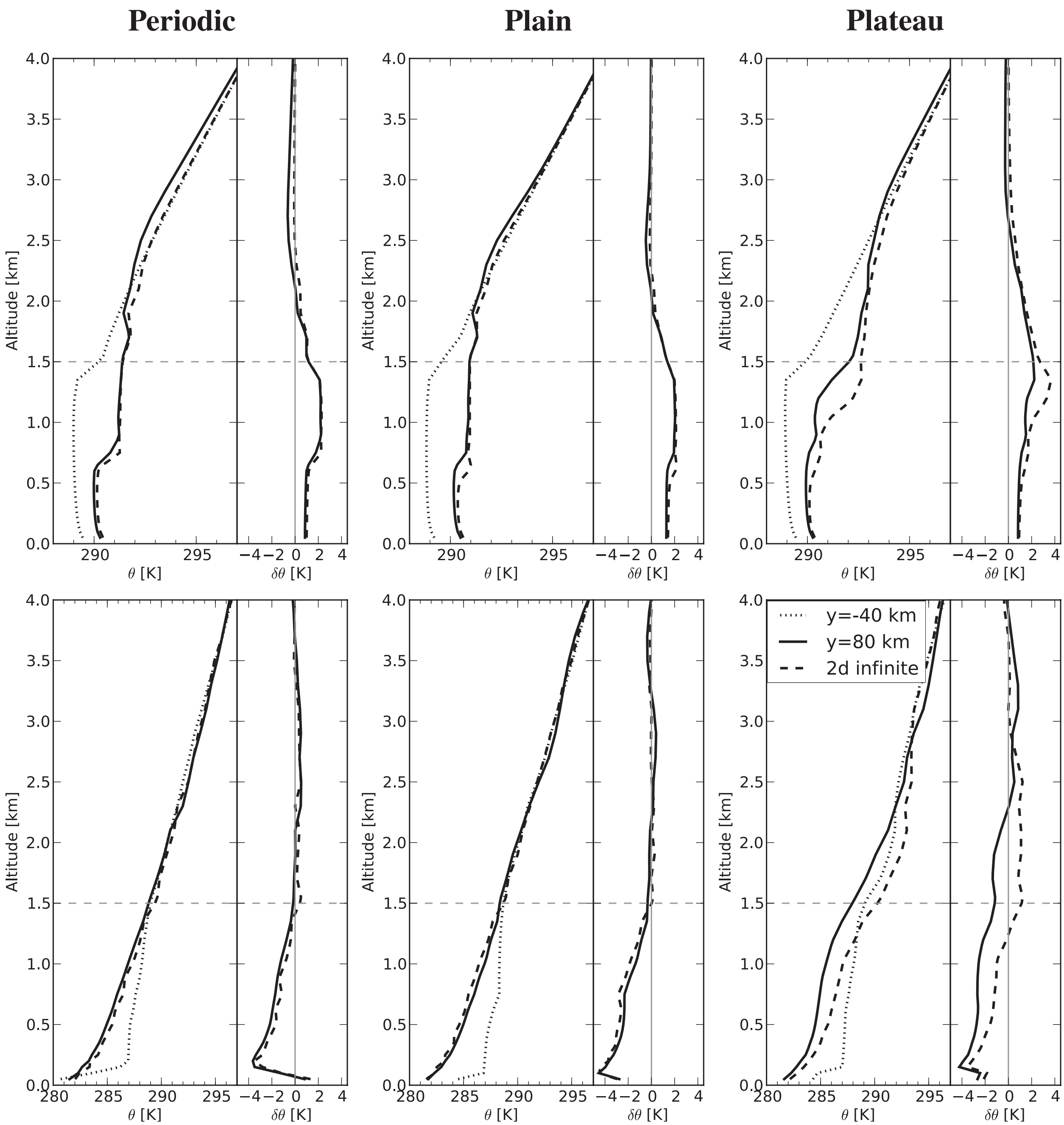

FIG. 11. Vertical profiles of potential temperature on the valley axis ($x = 0$) over the plain ($y = -40$ km) and in the valley ($y = 80$ km), and the valley–plain temperature difference $\delta\theta$, at (top) 1500 and (bottom) 0600 LT on the second day. Also included is the potential temperature profile for the corresponding infinite valley.

the along-valley winds, even in purely thermally driven situations.

Acknowledgments. The numerical simulations have been performed on the CRAY XT5 at the Swiss National Supercomputing Centre (CSCS) using the Advanced Regional Prediction System (ARPS) developed by the Center for Analysis and Prediction of Storms, University of Oklahoma.

REFERENCES

Catalano, F., and C.-H. Moeng, 2010: Large-eddy simulation of the daytime boundary layer in an idealized valley using the

Weather Research and Forecasting numerical model. *Bound.-Layer Meteor.,* **137,** 49–75.

De Wekker, S. F. J., S. Zhong, J. D. Fast, and C. D. Whiteman, 1998: A numerical study of the thermally driven plain-to-basin wind over idealized basin topographies. *J. Appl. Meteor.,* **37,** 606–622.

Egger, J., 1990: Thermally forced flows: Theory. *Atmospheric Processes over Complex Terrain, Meteor. Monogr.,* No. 45, Amer. Meteor. Soc., 43–58.

——, S. Bajrachaya, U. Egger, R. Heinrich, J. Reuder, P. Shayka, H. Wendth, and V. Wirth, 2000: Diurnal winds in the Himalayan Kali Gandaki Valley. Part I: Observations. *Mon. Wea. Rev.,* **128,** 1106–1122.

Gohm, A., and Coauthors, 2009: Air pollution transport in an alpine valley: Results from airborne and ground-based observations. *Bound.-Layer Meteor.,* **131,** 441–463.

Li, J. G., and B. W. Atkinson, 1999: Transition regimes in valley airflows. *Bound.-Layer Meteor.,* **91,** 385–411.

McKee, T. B., and R. D. O'Neil, 1989: The role of valley geometry and energy budget in the formation of nocturnal valley winds. *J. Appl. Meteor.,* **28,** 445–456.

McNider, R. T., and R. A. Pielke, 1984: Numerical simulation of slope and mountain flows. *J. Climate Appl. Meteor.,* **23,** 1441–1453.

Rampanelli, G., D. Zardi, and R. Rotunno, 2004: Mechanisms of up-valley winds. *J. Atmos. Sci.,* **61,** 3097–3111.

Rotach, M. W., and Coauthors, 2004: Turbulence structure and exchange processes in an alpine valley: The Riviera project. *Bull. Amer. Meteor. Soc.,* **85,** 1367–1385.

——, M. Andretta, P. Calanca, A. P. Weigel, and A. Weiss, 2008: Boundary layer characteristics and turbulent exchange mechanisms in highly complex terrain. *Acta Geophysica,* **56,** 194–219.

Schmidli, J., and R. Rotunno, 2010: Mechanisms of along-valley winds and heat exchange over mountainous terrain. *J. Atmos. Sci.,* **67,** 3033–3047.

——, G. S. Poulos, M. H. Daniels, and F. K. Chow, 2009: External influences on nocturnal thermally driven flows in a deep valley. *J. Appl. Meteor. Climatol.,* **48,** 3–23.

——, and Coauthors, 2011: Intercomparison of mesoscale model simulations of the daytime valley wind system. *Mon. Wea. Rev.,* **139,** 1389–1409.

Serafin, S., and D. Zardi, 2010: Daytime heat transfer processes related to slope flows and turbulent convection in an idealized mountain valley. *J. Atmos. Sci.,* **67,** 3739–3756.

Steinacker, R., 1984: Area–height distribution of a valley and its relation to the valley wind. *Contrib. Atmos. Phys.,* **57,** 64–71.

Wagner, A., 1938: Theorie und Beobachtung der periodischen Gebirgswinde. *Gerlands Beitr. Geophys.,* **52,** 408–449.

Weigel, A. P., F. K. Chow, and M. W. Rotach, 2007: On the nature of turbulent kinetic energy in a steep and narrow alpine valley. *Bound.-Layer Meteor.,* **123,** 177–199.

Whiteman, C. D., and J. C. Doran, 1993: The relationship between overlying synoptic-scale flows and winds within a valley. *J. Appl. Meteor.,* **32,** 1669–1682.

Xue, M., K. K. Droegemeier, and V. Wong, 2000: The Advanced Regional Prediction System (ARPS)—A multi-scale nonhydrostatic atmospheric simulation and prediction model. Part I: Model dynamics and verification. *Meteor. Atmos. Phys.,* **75,** 161–193.

——, and Coauthors, 2001: The Advanced Regional Prediction System (ARPS)—A multi-scale nonhydrostatic atmospheric simulation and prediction model. Part II: Model physics and applications. *Meteor. Atmos. Phys.,* **76,** 143–165.

Zängl, G., and S. G. Chico, 2006: The thermal circulation of a grand plateau: Sensitivity to the height, width, and shape of the plateau. *Mon. Wea. Rev.,* **134,** 2581–2600.